Phase Stability and Phase Transformations in Plutonium and Plutonium-Gallium Alloys

JEREMY N. MITCHELL, MARIUS STAN, DANIEL S. SCHWARTZ, and CARL J. BOEHLERT

The complexity of phase stability and transformations in plutonium alloys is reflected in the plutonium-gallium (Pu-Ga) phase diagram, which is perhaps the most complex of all binary systems. Although many investigations have explored phase equilibria, transformation systematics, and structure/property relations in the Pu-Ga system, many outstanding problems remain and new issues regularly appear. In this article, we describe recent dilatometry and calorimetry measurements on pure plutonium and plutonium-gallium alloys. We also present recent phase diagram modeling that attempts to unravel differences between the U.S. and Russian Pu-Ga phase diagrams. The ultimate goal of this work is to produce the first internally consistent database of thermophysical properties of this system so that a true equilibrium phase diagram can be produced and so that stability can be predicted over a range of conditions.

I. INTRODUCTION

UNDERSTANDING the stability of plutonium (Pu) and its alloys has been a scientific challenge since the early days of the Manhattan Project. This challenge is best represented by the six allotropes that pure Pu forms from room temperature to melting. These phases all have distinctly different crystal structures with significantly different cell volumes that are easily distinguished using a variety of *in-situ* analytical techniques, such as dilatometry and differential scanning calorimetry (Figure 1). Perhaps the most astonishing aspect of these allotropes is that the room-temperature phase, α, has the low symmetry monoclinic structure yet is the highest density phase. Alpha Pu is hard and brittle, making it difficult to machine. Addition of ~1 at. pct Ga will stabilize the softer face-centered cubic δ phase, which has proven to be technologically the most useful allotrope. Stabilization of δ phase presents additional complexities to plutonium, such as the appearance at low temperatures of the martensitic α' phase, the effects of aging on δ stability, and the sensitivity of physical properties to solute addition. Recent focus on the Russian Pu-Ga phase diagram and its differences with the more widely accepted U.S. diagram is an important example of the elusive nature of our knowledge of phase stability in plutonium alloys (Figure 2).[1]

In this article, we will highlight recent dilatometry and calorimetry experiments on stability and transformations in pure Pu and Ga-stabilized δ Pu. In particular, we are studying the effects of composition, microstructure, and age on the stability of these materials. The intent of these experiments is to develop a comprehensive and internally-consistent database of the thermophysical and transformation properties of Pu-Ga alloys. We will also discuss recent phase diagram modeling of the Pu-Ga system, the purpose of which is to assess differences between the U.S. and Russian phase diagrams.

II. PLUTONIUM ALLOY STABILITY DURING THE MANHATTAN PROJECT

In light of the sixtieth anniversary of the creation of the predecessor of Los Alamos National Laboratory, we thought it appropriate to review the earliest observations of phase stability in plutonium and its alloys based on the accumulated observations of Edward Hammel.[2] Metallic plutonium was first produced in November 1943 at the University of Chicago's Met Lab as part of the early stages of the Manhattan Project. Measured densities of these samples were 15.4 g/cc. Subsequent metallic spheres had densities between 13 and 21 g/cc, and this was the first indication of the complexities of phase stability in plutonium. This issue was the first major task facing the Los Alamos Plutonium Metallurgy Group, and in May 1944, enough evidence had been produced to link this density variability with allotropism. Two phases were identified: a high-temperature, relatively soft phase with a density of ~16 g/cc, and an ambient temperature, brittle phase with a density of ~20 g/cc. These two phases, β and α, respectively, were definitively identified using dilatometry in June 1944. Soon after, the γ and δ phases were identified and the transition temperatures of the four allotropes were fairly well bracketed using thermal analysis. These early experiments also first highlighted the striking reversion hysteresis for these thermal transformations. Quantitative studies of physical properties of the allotropes continued through September 1944 and included measurements of thermal expansion coefficients, phase transformation rates, X-ray diffraction, tensile strength, ductility, and hardness. During these experiments, it was determined that α Pu was too hard and brittle for rolling or pressing and that β phase had a much more favorable processing behavior. Upon cooling, however, samples worked in the β stability field cracked or distorted significantly.

JEREMY N. MITCHELL, and DANIEL S. SCHWARTZ, Technical Staff Members, Nuclear Materials Technology Division, and MARIUS STAN, Technical Staff Member, Materials Science and Technology Division, are with the Los Alamos National Laboratory, Los Alamos, NM 87545. Contact e-mail: jeremy@lanl.gov CARL J. BOEHLERT, Assistant Professor, Department of Ceramic Engineering and Materials Science, Alfred University, Alfred, NY 14802, is also with the Nuclear Materials Technology Division, Los Alamos National Laboratory.

This article is based on a presentation in the symposium "Terence E. Mitchell Symposium on the Magic of Materials: Structures and Properties" from the TMS Annual Meeting in San Diego, CA in March 2003.

In October of 1944, Cyril Stanley Smith, the Associate Division Leader for Metallurgy, suggested that the solution to the cracking problem of worked metal might be found in alloying plutonium with small amounts of other elements. This was attributed to the inadvertent Pu-Fe, −Ni, and −Cu alloys formed in June 1944 during attempts to remelt plutonium in various metal crucibles. The initiation of the Alloy Research Program was critical to the success of the Manhattan Project and began with the preparation of a series of binary and a few multicomponent alloys. The initial binaries included Pu-Al, -Be, -C, -Fe, -Li, -Mn, -Th, and -U, and the multicomponent alloys contained Pu-Co-Ni, -Pt-Ir, -Mg-Cd-Zn, -Pb-Sn-Ge-Si, -Ti-V-Cr-Mo-Zr, and -Fe-Co-Ni. Solute concentration was limited to 1 at. pct of each element in each alloy. Of these alloys, Pu-1 at. pct Al maintained the high-temperature δ phase density at room temperature. The reliability of this alloy was well established before December 1944, when a comprehensive series of Pu-Al alloys was made to evaluate the effects of composition on stability and physical properties. However, physics-based impurity guidelines on alloy purity set the maximum content of Al at 910 wppm, or 0.5 at. pct. This tolerance is a function of the collision of α particles with an impurity nucleus and the production of neutrons from (α, n) reactions. The resulting neutron background increases the chance of initiating a fission chain reaction well before the planned postfiring condition of maximum criticality is attained. This results in a predetonation in which little of the active material fissions before the entire assembly is blown apart.

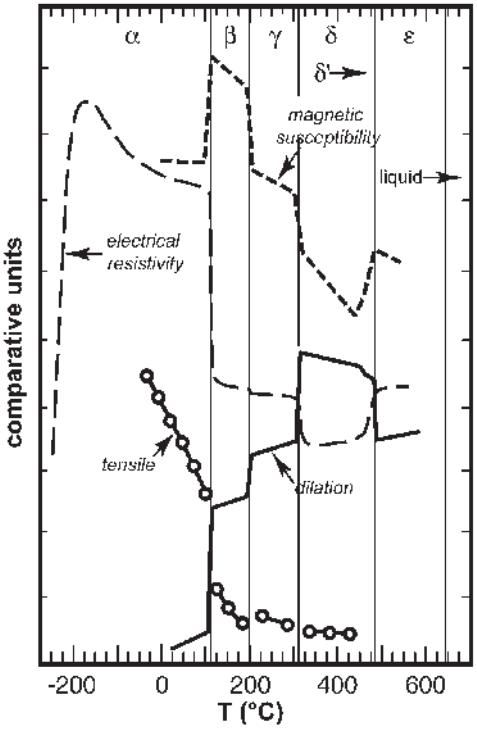

Fig. 1—Selected physical properties of pure Pu as a function of temperature.

The establishment of stricter purity tolerances in March 1945 meant that the prime δ-stabilization candidate was no longer acceptable. A suggestion to look at related elements led to subsequent studies of Si and Ga alloys, and these proved to be suitable δ-phase stabilizers. Gallium became the favored δ stabilizer because its higher atomic number meant that its (α, n) yield was negligible. Therefore, the remarkably stable Pu-1 at. pct Ga alloy was selected for more intense scrutiny. Interestingly, it was realized during May 1945 that there was no theoretical or experimental basis for believing that this alloy was thermodynamically stable. This resulted in dilatometer studies of up to 220 hours to assess stability as a function of time and temperature. Additional tests using cold working followed by deformation of up to 200 ksi to induce transformation

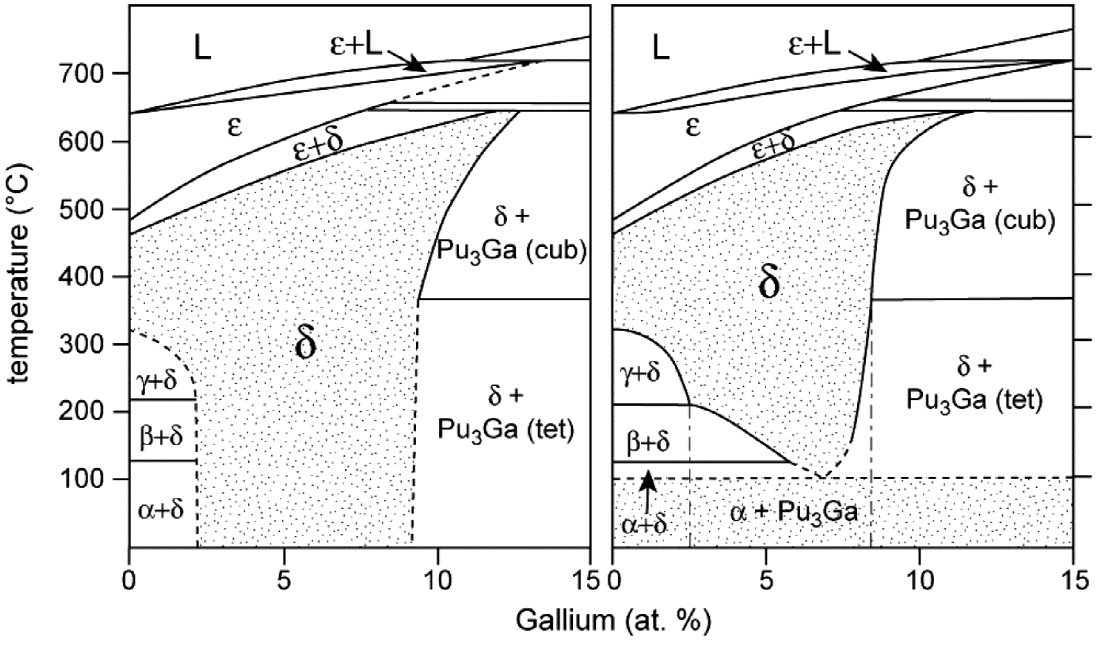

Fig. 2—Comparison of the low-Ga region of the Pu-Ga phase diagram published by American[10] (left) and Russian[20] (right) researchers. Note the smaller size of the δ field and the presence of the α + Pu_3Ga field in the Russian diagram.

validated the stability of this alloy. Density was monitored in several samples for 44 days with no evidence of instability. Finally, on July 1, 1945, the plutonium hemispheres for the Trinity Test were completed and delivered.

Following the Manhattan Project, phase stability was investigated at Los Alamos, Rocky Flats, Hanford, and the Lawrence Livermore National Laboratory throughout the Cold War. Parallel work was undertaken in the former USSR, as well as in England and France. Plutonium research slowed in the mid to late 1980s as a result of bans on underground nuclear testing and the end of the Cold War, and funding levels dropped precipitously. Ironically, significant improvements in analytical equipment, largely made possible by the computing technology explosion, occurred during the same time period. Recent work at Los Alamos, Livermore, and in France represents the first use of modern technology to understand phase transformations and stability.

III. MICROSTRUCTURAL INFLUENCES ON PHASE STABILITY

Intragranular distribution of Ga is the most important factor influencing stability in Pu-Ga alloys. To illustrate the effect of Ga microsegregation, the compositional path of a crystallizing grain of Pu-1 wt pct Ga is depicted in Figure 3. Starting at A, the grain is completely ε as it cools toward the upper boundary of the $\delta + \varepsilon$ field. Once the boundary is reached, Ga-rich δ phase begins to crystallize. As the grain cools through the two-phase field, the Ga content of δ decreases (B) toward the bulk composition of the alloy and the remaining ε becomes increasingly deficient in Ga (C). Once the grain passes through the lower boundary of the two-phase field, it has completely transformed to δ (D). Coring in δ grains is preserved due to the comparatively slow interdiffusion of Ga in δ Pu as compared to that in ε. Although the phase diagram predicts coring as a grain cools through the ε + liquid field, diffusion is so rapid in ε Pu that the solid essentially homogenizes instantaneously. The magnitude of the coring remaining at room temperature reflects the difference in $\widetilde{D}^{Ga}_{Pu}$ between the ε and δ phases. $\widetilde{D}^{Ga}_{\delta Pu}$ is four to seven orders of magnitude slower than $\widetilde{D}^{Ga}_{\varepsilon Pu}$ (10^{-14} to 10^{-11} and 10^{-8} to 10^{-7} $cm^2\ s^{-1}$, respectively), suggesting that the coring preserved in microsegregated alloys occurs during the solid-state transformation rather than during solidification. Furthermore, diffusion in δ Pu is slow enough that the distribution of Ga occurring upon transformation to the δ phase can be calculated from the equilibrium phase diagram.[3]

An as-cast Ga-poor alloy is a composite consisting of laths of δ Pu in a matrix of α Pu. An example of the as-cast cored microstructure in a sample of Pu-0.6 wt pct Ga is shown in Figure 4. Grain size is dependent on cooling rate, and there is a tendency to produce slightly more acicular and euhedral grains with increasing cooling rate.[3,4] There are three distinct regions within a cored sample: (1) Ga-rich δ phase in the cores of grains; (2) Ga-poor, metastable, δ phase outer shell surrounding the grain cores, and (3) low Ga α phase matrix. The light-colored areas within the distinct grains in Figure 4 represent region 1. The darker areas at the edges of each grain are region 2, whereas the light matrix represents region 3. For a Pu-1 wt pct Ga alloy, the Ga-rich core of a grain typically contains ~1.5 to 1.6 wt pct Ga and the grain boundary has essentially no Ga (below the detection limits of electron microprobe analysis). Most of the change in Ga concentration occurs in the outer 15 pct (by area) of a typical Pu grain. This reflects the fact that the first 10 vol pct of a growing sphere accounts for ~45 pct of its final radius, whereas the last 10 vol pct is concentrated in the outer 4 pct of the radius.[3]

The as-cast microstructure is compositionally homogenized using thermal processing at temperatures within the δ phase

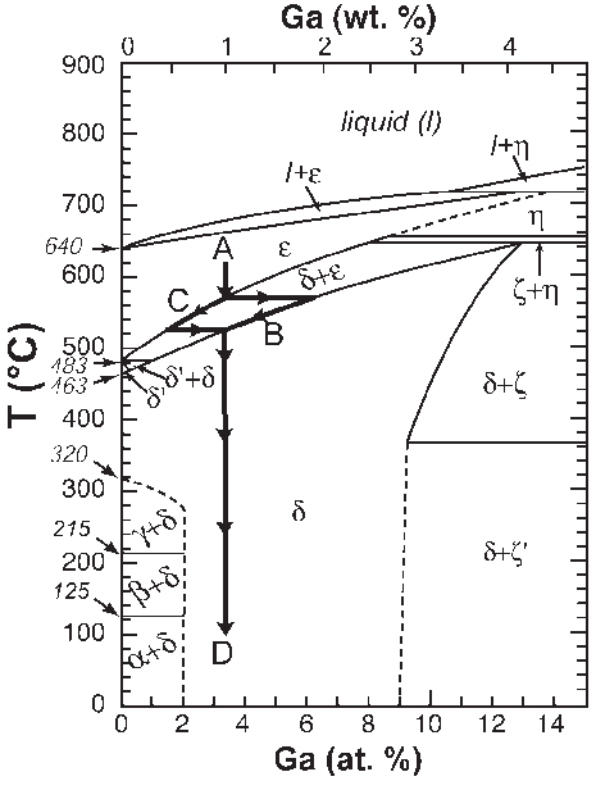

Fig. 3—Crystallization path of a Pu-1.0 wt pct Ga alloy.

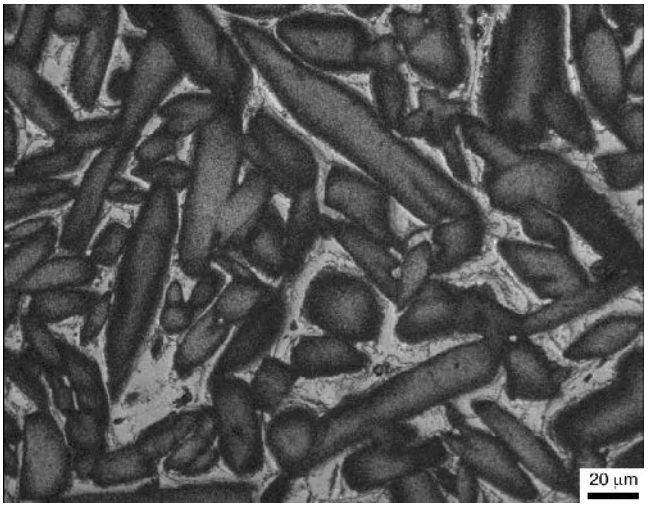

Fig. 4—Optical photomicrograph of an as-cast Pu-0.6 wt pct Ga alloy. Note the laths of δ Pu within the matrix of α Pu. Gray-scale variation within the δ grains reflects Ga zonation, with darker Ga-poor rims and lighter Ga-rich cores (image 01-009-20-500).

region (380 °C to 480 °C). Annealing eventually results in the homogeneous distribution of Ga within grains and throughout the sample. This process generally requires ~100 hours for complete homogenization at temperatures of ~450 °C.[5] The sample shown in Figure 5 was annealed for 50 hours at 420 °C and the gray-scale variations within grains indicates that there is still significant compositional zonation of Ga.

IV. EXPERIMENTAL METHODS

Samples analyzed in this study include high-purity zone-refined α Pu[6] and electrorefined Pu-Ga alloys. Phase and compositional homogenization was accomplished by wrapping the samples in Ta foil, encapsulating in glass, and annealing in a furnace at 420 °C or 450 °C for 100 hours. Following homogenization, one sample was cold rolled to 91 pct reduction followed by annealing at 350 °C for 15 minutes. Plutonium samples were cut using a slow-speed saw and the surfaces were ground parallel and polished. Special attention was paid to removing surface Pu oxide. Samples for differential scanning calorimetry (DSC) were punched using a 3-mm transmission electron microscopy (TEM) sample disk punch. Dilatometry samples typically weighed from 200 to 400 mg and the thickness ranged from 750 to 2000 μm · DSC samples weighed from 15 to 25 mg.

Dilatometry experiments were performed using a Linseis (Selb, Germany) L70 low-temperature horizontal dilatometer and a Netzsch (Selb/Bayern, Germany) 402C dilatometer with a low-temperature furnace. Both systems use quartz glass samples holders and pushrods. Cooling and heating rates were 2.5 °C/min to 5 °C/min. Cryogenic experiments on both systems used flowing filtered He gas flowing at 30 to 50 mL/min; the Netzsch system was evacuated and backfilled with He prior to gas flow. Typical pushrod load on the sample was 25 mN. Analysis of NIST stainless steel, copper, and borosilicate glass standards were within ~2 pct of accepted values.

Calorimetry was performed using a Perkin-Elmer (Boston, MA) Pyris-1 power compensation DSC. Heating and cooling rates of 10 °C/min were used. The calorimeter furnace was purged with flowing, ultrahigh purity Ar gas at 20 mL/min. Specimens were hermetically sealed into standard Al pans prior to thermal scanning. Calibration of the instrument was done using the two-point In/Zn method; calibrations were tested by melting Sn. The Sn melt onset temperature was typically within ~0.05 pct, and the enthalpy of melting within ~1.0 pct of standard values.

V. EXPERIMENTAL RESULTS

A. *Zone-Refined Alpha Pu*

Dilatometric heating and cooling traces for zone-refined Pu are shown in Figure 6. All transformations occurred within ~5 °C of those measured using DSC (Table I). The characteristic negative thermal expansion of δ is not evident,

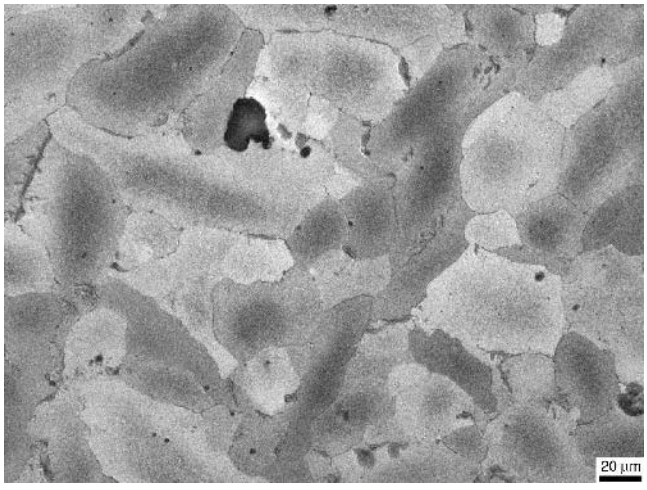

Fig. 5—Photomicrograph of a Pu-0.6 wt pct Ga alloy after annealing for 50 h at 420 °C. No α is present, but gray-scale zonation indicates that the sample is still not homogenized with respect to Ga (image 01-054-067-500).

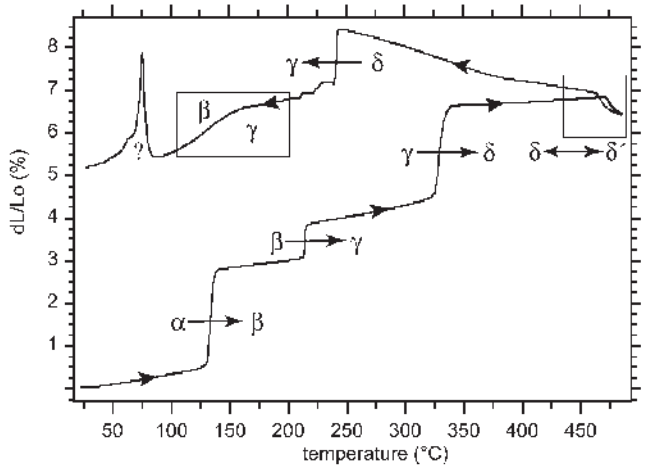

Fig. 6—Dilatometry of zone-refined α Pu from room temperature to 480 °C. Note the significant hysteresis of the reverse transformations. The slight positive expansion within the δ field and the large difference between initial and final sample lengths probably reflect *in-situ* oxidation of the sample.

Table I. Onset Temperatures and Enthalpies of Phase Transformations in Pure Plutonium from This Study and Ward[19]

Transformation	Onset Temperature (°C)			Enthalpy	
	Ward[19]	Dilatometry	DSC	This Study	Ward[19]
$\alpha \rightarrow \beta$	124.6	131.1	126	15.43	15.50
$\beta \rightarrow \gamma$	214.8	213.6	214	2.18	2.00
$\gamma \rightarrow \delta$	320.0	325.6	323	2.35	2.98
$\delta \rightarrow \delta'$	463.0	472.1	468	0.27	0.35
$\delta' \rightarrow \varepsilon$	482.6	—	486	7.16	7.00
$\varepsilon \rightarrow$ liquid	124.6	—	—	—	—

which may be due to oxidation of the sample at this high-temperature range. The maximum temperature of the experiment was just short of the $\delta' \rightarrow \varepsilon$ transformation. Significant hysteresis is evident in the reverse transformation, with displacement becoming progressively larger during cooling. The $\delta \rightarrow \gamma$ and $\gamma \rightarrow \beta$ reversions are distinctly different from their heating transformations, which may be due to oxidation but seems more likely to be related to mechanisms and kinetics of the reversion. A final *dL/L* peak is evident close to room temperature, which may be due to cracking of the oxide layer. The final length change difference may reflect the approximate thickness of this oxide layer, the retention of a high-temperature phase, or a combination of these possibilities.

The onset temperatures for transformations in pure Pu measured using DSC in this study are listed in Table I. The agreement with literature values is reasonable, although in general the onset temperatures are in better agreement than the enthalpies. The variation in transition enthalpies seen in the literature is likely to be the result of different impurity levels, which can have a large effect on enthalpy. The high purity of the Pu used here adds confidence to the thermodynamic parameters measured in this study. Figure 7(a) shows a typical DSC heating scan for pure Pu. On heating, the transitions are all narrow, well-defined endothermic events, as expected for allotropic phase transformations. However, on cooling (Figure 7(b)), several of the reverse transformations show unusual behavior. The cooling transformations are summarized in Table II. The $\varepsilon \rightarrow \delta'$ and $\delta' \rightarrow \delta$ transformations are normal, looking like exothermic versions of the heating transformations, with normal amounts of undercooling. However, the $\delta \rightarrow \gamma$ transformation shows a completely different behavior, as seen in the insert in Figure 7(b). This was observed using dilatometry about 40 years ago,[7] but this study is the first quantification of the calorimetric aspects of the transition. Rather than a single, well-defined heat release, the transformation occurs as a series of distinct heat spikes spread over the 260 °C to 180 °C temperature range. In general, the first spikes to occur are the largest in magnitude, and each subsequent heat release is smaller as the specimen cools. The appearance of the $\delta \rightarrow \gamma$ cooling transformation is consistent with the transformation being strain controlled (*i.e.*, martensitic), and this is being studied further.[6] If the total enthalpy of the $\delta \rightarrow \gamma$ transformation is calculated by summing the enthalpy of each of the individual heat spikes over the 260 °C to 180 °C range, it is found to be about 25 pct lower than the magnitude of the $\gamma \rightarrow \delta$ heating transformation. This suggests that a significant amount of δ may be retained to low temperatures, or that the martensitic $\delta \rightarrow \gamma$ transformation is less energetic than the conventional $\gamma \rightarrow \delta$ heating transformation. The subsequent cooling transformations, $\gamma \rightarrow \beta$ and $\beta \rightarrow \alpha$, also show lower enthalpy than their associated heating transformations, which supports the possibility of retained phases. The $\gamma \rightarrow \beta$ cooling transformation also is significantly different than its heating counterpart. First, the cooling transformation has an undercooling of >100 °C relative to the heating transformation, an unusually large amount. Second, the cooling transformation is much broader. On heating, the $\beta \rightarrow \gamma$ transformation completes in <10 °C, while the reverse cooling transformation requires 30 °C to complete at the same 10 °C/min temperature scanning rate. The extreme asymmetry observed between the heating and cooling transformations for the $\beta \rightarrow \gamma/\gamma \rightarrow \beta$ and $\gamma \rightarrow \delta/\delta \rightarrow \gamma$ transformations is not presently understood.

B. *Pu-Ga Alloy*

Most of the dilatometric experiments use the onset of the martensitic $\delta \rightarrow \alpha'$ transformation (M_s) and the complementary reversion to monitor the influence of composition

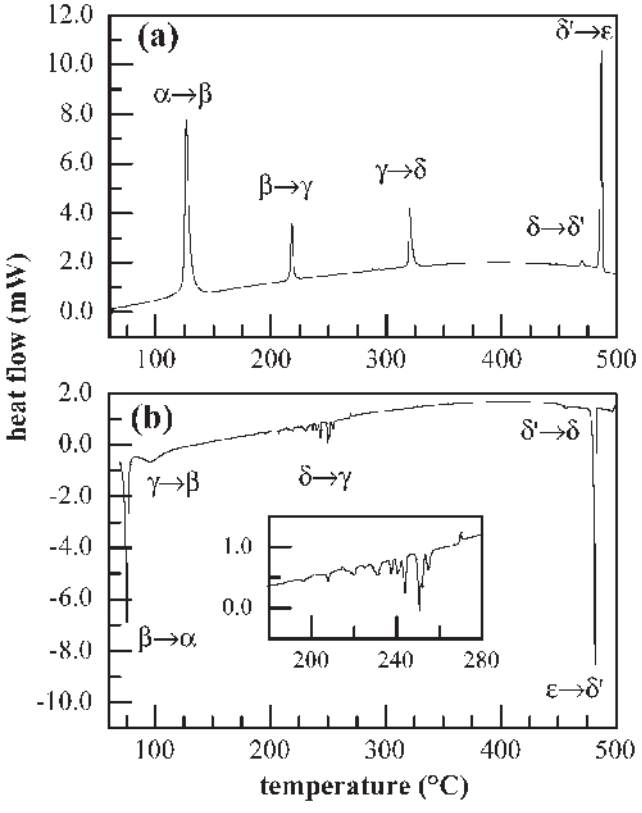

Fig. 7—(*a*) Heating and (*b*) cooling DSC scans for pure Pu. The insert in (b) shows the martensitic $\delta \rightarrow \gamma$ transformation in more detail.

Table II. Transformation Onset Temperatures and Enthalpies Measured by DSC during Cooling from the ε Phase Field

Transformation	Onset Temperature (°C)	ΔH	Comments
$\varepsilon \rightarrow \delta'$	483.911	−7.1215	—
$\delta' \rightarrow \delta$	461.199	−0.222	—
$\delta \rightarrow \gamma$	260 to 180	−2.1405	martensitic transformation
$\gamma \rightarrow \beta$	113.624	−1.7225	unusually broad
$\beta \rightarrow \alpha$	78.278	−10.4685	scan ended before transformation complete, ΔH is significantly underestimated

Table III. $\delta \rightarrow \alpha'$ Transformation and Reversion Temperatures of Various Alloys

Ga Content (Wt Pct)	Processing Parameters	Thermal Cycles	M_s* (°C)	M_s2** (°C)	M_f† (°C)	R_s‡ (°C)	R_f§ (°C)	Maximum α' (Pct)
0.6	50 h, 420 °C	1	−126.2	—	—	44.8	100.0	12
0.6	100 h, 420 °C	1	−118.7	—	—	43.9	99.6	19
0.5	50 h, 430 °C	1	−111.7	−96.3	−66	91.7	115.7	24
0.6	100 + h, 420 °C; rolled to 91 pct reduction	1	−144.9	—	—	48.3	66.9	16
0.6	100 h, 420 °C; rolled to 91 pct reduction	3	−154.7¶	—	—	38.2	72.5	5

*Martensite start.
**Martensite reinitiation.
†Martensite finish.
‡Reversion start.
§Reversion finish.
¶Transformation occurred after 16 min hold at ~−155 °C.

and microstructure on phase stability. These results are summarized in Table III. For simplicity, only the most relevant portions of dilatometric traces are shown.

1. *Bulk composition*

Compositional effects on stability are fairly well known, and lower Ga contents lead to a predictably smaller δ stability field.[8] Figure 8 shows partial results of experiments on 0.5 and 0.6 wt pct Ga alloys. Although the starting materials have different origins, they have similar thermal histories and intragranular Ga distribution. The martensite start temperature (M_s) for the 0.5 wt pct Ga alloy is −111.7 °C, in comparison to −126.2 °C for the 0.6 wt pct sample. The pre-transformation contraction is slightly greater in the latter sample. Following an isothermal hold at −155 °C, the 0.6 wt pct alloy expands as it warms to room temperature, and the reversion starts (R_s) and ends (R_f) at 44.8 °C and 100.0 °C, respectively. In contrast, the 0.5 wt pct alloy has a transformation reinitiation (M_s 2) during warming at −96.3 °C that ends at −66.0 °C (M_f). The reversion begins at 91.7 °C and finishes at 115.7 °C. Detailed evaluation of the reversion in the 0.5 wt pct sample in Figure 9 shows the martensitic nature of the reversion, which is characterized by a series of bursts in *dL/dt* over a narrow temperature range. This experiment appears to be the first time this phenomenon has been observed, and we have seen it in subsequent samples of similar bulk composition and in poorly homogenized samples.

A photomicrograph of a partially transformed Pu-0.6 wt pct Ga alloy is shown in Figure 10. This is the same material as shown in Figure 5 but was cooled to −155 °C, held for 1 hour, and warmed to room temperature. The fine, light colored laths are α' in a matrix of δ Pu. These platelets tend to be concentrated in low-Ga regions that appear dark compared to the Ga-rich cores. Three primary orientations of the platelets are visible, and a detailed analysis of the α'-δ orientation relationship can be found in Zocco *et al.*[9]

The DSC is a sensitive probe for the degree of homogenization that a Pu-Ga alloy has undergone. Pu-Ga alloys with >0.5 wt pct Ga that have been carefully homogenized in the δ-phase field will remain δ at room temperature essentially indefinitely. However, if regions of the material have Ga concentration below ~0.2 wt pct Ga, as can easily be the case in Pu-Ga alloys with 0.4 to 1.0 wt pct Ga due to the coring phenomenon, these low-Ga areas will transform to α below ~100 °C. Figure 11 shows a typical DSC scan for a cored

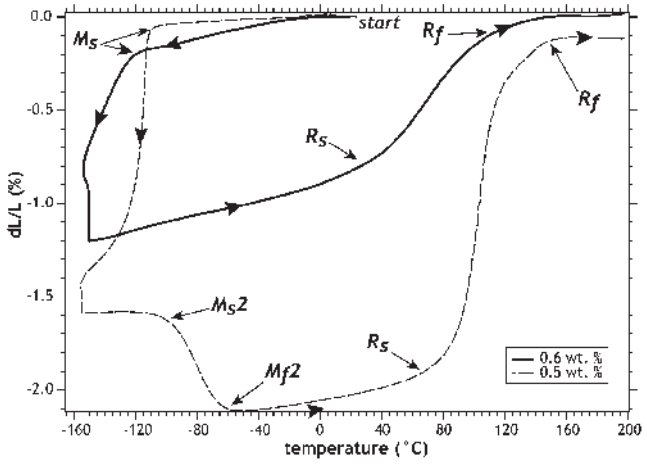

Fig. 8—Dilatometric comparison of the $\delta \rightarrow \alpha'$ transformation and reversion in Pu-0.5 wt pct Ga and Pu-0.6 wt pct Ga alloys. Both samples were annealed at 420 °C for 50 h to minimize Ga concentration variations. Note the reinitiation of the transformation in the former sample during warming.

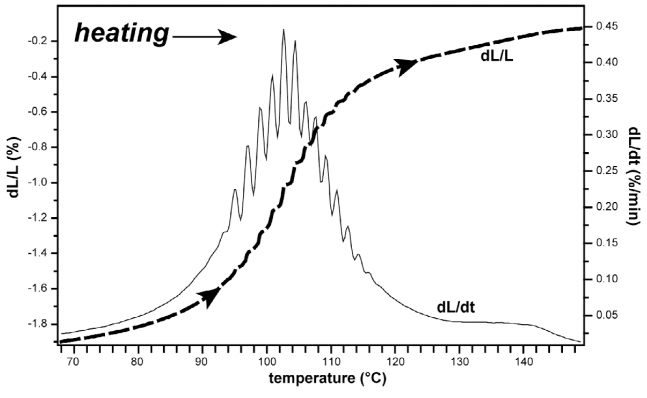

Fig. 9—Detail of the $\alpha' \rightarrow \delta$ reverse transformation in Pu-0.5 wt pct Ga. Analysis of *dL/dt* shows the martensitic nature of the reversion, which is characterized by a series of bursts.

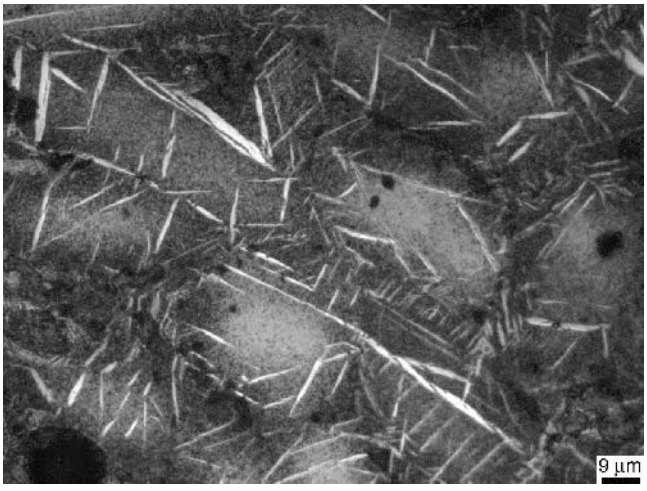

Fig. 10—Optical photomicrograph of a Pu-0.6 wt pct Ga alloy following cooling to −155 °C, holding for 60 min, and warming to RT. Note the light-colored laths of α' Pu within the δ Pu matrix (image 01-036-33L-1000).

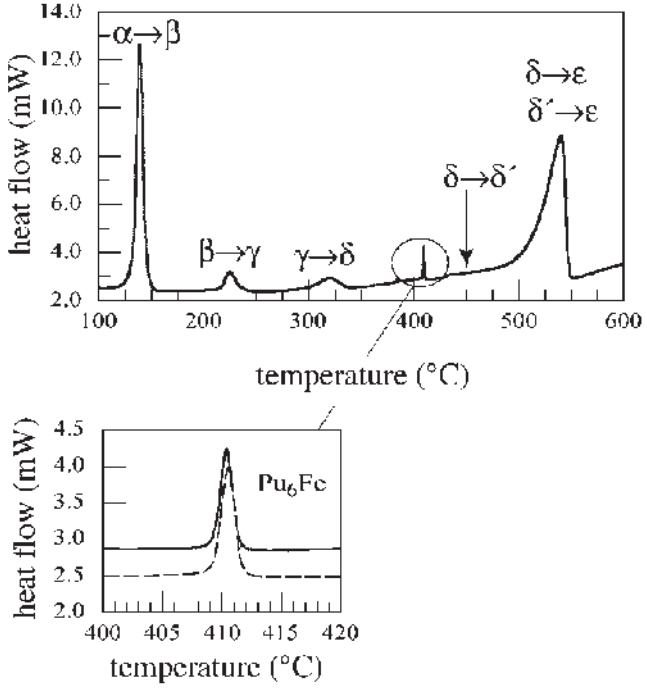

Fig. 11—DSC heating scan for a Pu-0.6 wt pct Ga alloy.

Pu-0.6 wt pct Ga alloy, and the endothermic peaks for the $\alpha \rightarrow \beta$, $\beta \rightarrow \gamma$, and $\gamma \rightarrow \delta$ transformations are readily apparent. While the specimen used to make the scan in Figure 11 contained a relatively large amount of α, DSC is sensitive enough to detect as little as 0.1 vol pct α in a δ matrix by measuring the $\alpha \rightarrow \beta$ transformation heat absorption. A side effect of inhomogeneous Ga distribution is that at temperatures above ~325 °C, there are two types of δ phase present, primary and secondary. The primary δ has Ga content high enough that it remains stable down to room temperature. The secondary δ is low enough in Ga, due to coring, to transform to α at room temperature. This α then transforms through the β and γ phases during reheating to the δ-phase field. Some of the secondary δ has a low enough Ga content that it was

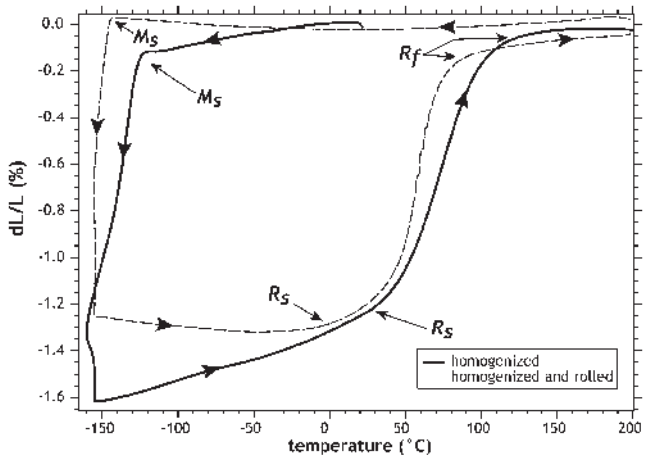

Fig. 12—Comparison of the dilatometric response of an as-homogenized Pu-0.6 wt pct alloy and the same material that has been rolled to reduce grain size (30 and 17 μm, respectively).

observed to transform to δ', indicating that some of the cored δ was very low in Ga, probably <0.1 wt pct (it is believed that very low levels of impurities or alloying additions will preclude the δ' phase from forming). At ~520 °C, both the low-Ga δ' and the higher-Ga δ transform together to the ε phase. The presence of Fe in Pu-0.5 wt pct Ga alloys above ~200 wppm causes the formation of the relatively low-melting intermetallic compound Pu_6Fe. The endothermic melt peak for this compound can be easily seen in Figure 11. The exact temperature at which this compound melts depends sensitively upon the exact Pu-Ga-Fe composition, but it is precisely repeatable over subsequent reheats for a given alloy.

2. *Grain size*

Reduced grain size generally suppresses the start of a martensitic transformation. This effect is apparent in Figure 12, where the rolled and finer-grained sample (17 μm) has a much lower M_s (−144.9 °C) than its unrolled and coarser-grained (30 μm) parent material (−118.7 °C). Interestingly, the rolled sample has an unusual pretransformation expansion during cooling, unlike its parent. The transformation is much sharper in the rolled sample, but the pct *dL/L* is greater in the coarse-grained sample (19 pct *vs* 16 pct α). Also, the rolled sample is essentially invariant during warming prior to reversion, whereas the other sample has a steady expansion prior to reversion. The reversion start and finish temperatures are 43.9 °C and 99.6 °C for the homogenized sample and 48.3 °C and 66.9 °C for the rolled sample.

We have also evaluated hysteresis in the $\delta \rightarrow \alpha'$ transformation in several samples. In general, cycling these samples through multiple thermal cycles, such as the ones depicted previously, result in progressive displacement of M_s to lower temperatures or longer times during an isothermal stage (Table III). This phenomenon is shown in Figure 13, where the rolled sample was thermal cycled three times. In this case, the first and third cycles are depicted. The onset of the $\delta \rightarrow \alpha'$ transformation is displaced from −144.9 °C for the first cycle to −154.7 °C after 16 minutes of holding at ~−155 °C for the third cycle. The amount of transformation is greatly reduced as a function of cycling, with the maximum *dL/L* dropping from ~−1.25 to ~−0.5 pct. The reversion is similarly effected by thermal cycling (Figure 14), with the *dL/Dt* of the third

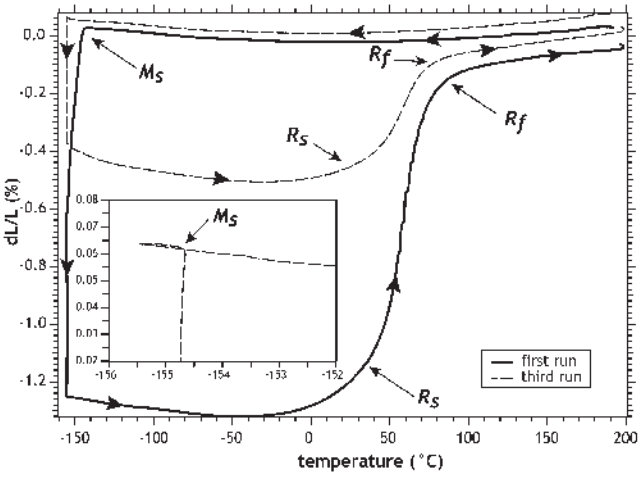

Fig. 13—Example of hysteresis in multiply thermal cycled samples as measured by dilatometry. The M_s becomes increasingly displaced to lower temperatures as a function of cycling.

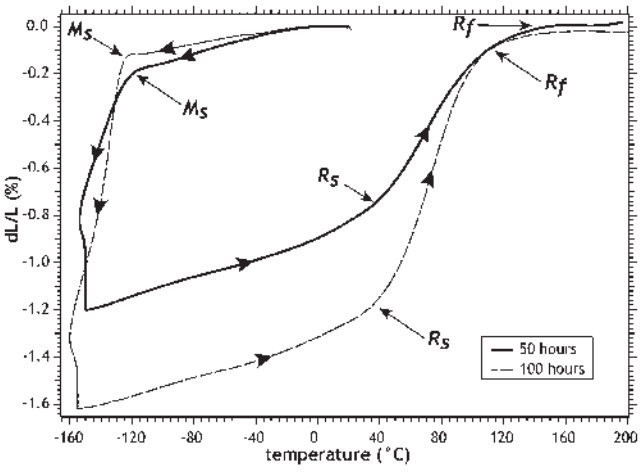

Fig. 15—Comparison of the $\delta \rightarrow \alpha'$ transformation in Pu-0.6 wt Ga samples that have been annealed for 50 and 100 h at 420 °C. Both microstructures are structurally homogenous, but variations in Ga distribution still affect transformation behavior in the 50-h sample.

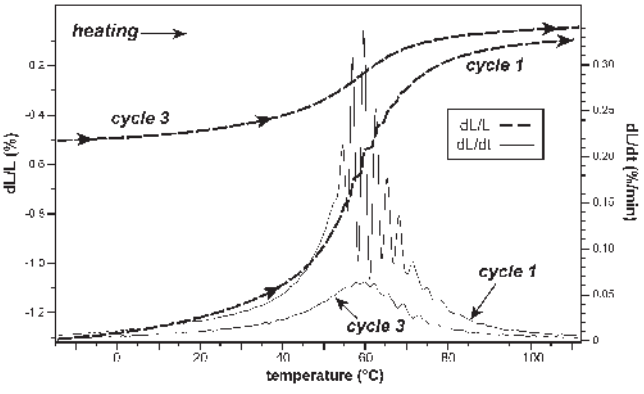

Fig. 14—Plot of *dL/L* (pct) and *dL/dt* (pct/min) in the same sample thermal cycled one and three times.

cycle having lower amplitude martensitic bursting features. The expansion coefficients are not affected by cycling, as evidenced by the parallel *dL/L* paths of the cycles. The temperature range of the reversion is ~16 °C larger for the third cycle.

3. *Ga distribution*

Sample splits taken from the same starting material were annealed at 420 °C for 50 and 100 hours. Both microstructures are fairly homogenous, with Ga ranging from 0.4 to 0.7 wt pct from the rim to the core of the grain in the 50-hour sample. The 100-hour sample has no systematic Ga concentration variation. The 50-hour sample has slightly more contraction during cooling, and the 100-hour has a more distinct transformation onset (Figure 15). The M_s for these samples are −126.2 °C and −118.7 °C, respectively. The amount of transformation is greater in the more homogenous material (19 pct *vs* 12 pct α'). They have similar expansion coefficients during warming from the cryogenic isothermal stage.

VI. MODELING METHODS AND RESULTS

Almost 40 years after Ellinger *et al.*[10] published the phase diagram of the Pu-Ga system, the stability in this system is still the subject of controversy. This diagram shows δ phase stable at room temperature for Ga concentrations between 2 and 8 at. pct (Figure 2). Hocheid *et al.* reported similar results in 1965.[11] The diagram proposed by Chebotarev *et al.* in 1975[12] sparked the debate by proposing a eutectoid decomposition of the δ phase into $\alpha + Pu_3Ga$ at 373 K (Figure 2). For many years, the presence of the eutectoid point was rejected based on normal pressure experimental results. Recently, Hecker and Timofeeva[1] revealed that Chebotarev *et al.* applied mechanical work to enhance the kinetics of the phase transformation to force the eutectoid decomposition. In 1986, Kassner and Peterson published an assessment of the Pu-Ga diagram that confirms the Ellinger diagram.[13,14] However, in 1991, Adler published a CALPHAD type assessment that is consistent with the Chebotarev *et al.* diagram.[15] Recently, a new approach was proposed for phase stability calculations[16] and was further developed to describe the Pu-Ga system.[17] It is based on atomistic potentials, such as the modified embedded atom method (MEAM), and molecular dynamics (MD) calculations. The results confirm the eutectoid decomposition.

Various data sets contribute to the thermodynamic modeling required to determine phase stability in multicomponent systems. The experimental results presented previously are a first step toward a self-consistent description of the thermodynamic properties. In the particular case of the Pu-Ga system, the database is still incomplete and the uncertainty of the thermodynamic values is large. Further experimental and theoretical results are necessary to accurately describe the properties of the system. We present here an assessment of the Pu-Ga diagram in the low-temperature and Ga content area, to emphasize the sensitivity of the phase stability with respect to the thermodynamic properties of components, compounds, and solutions.

In the experimental work, temperature T and pressure P are the intensive variables used to describe and control the thermodynamics of the system. The equilibrium state of the system corresponds to the minimum of the Gibbs free energy

$$G(T, P) = H - TS \qquad [1]$$

where H and S are the enthalpy and the entropy, respectively. The enthalpy is related to the internal energy E through the pressure P and the volume V:

$$H = E + PV \quad [2]$$

The enthalpy and the Gibbs free energy are related by

$$H(T) = G(T) - T\left[\frac{\partial G(T)}{\partial T}\right]_P \quad [3]$$

The knowledge of the free energy allows for the calculation of other important properties, at constant pressure, such as the entropy,

$$S(T) = -\left[\frac{\partial G(T)}{\partial T}\right]_P \quad [4]$$

The heat capacity,

$$C_p(T) = -T\left[\frac{\partial^2 G(T)}{\partial T^2}\right]_P = \frac{\partial H(T)}{\partial T} \quad [5]$$

and the linear thermal expansion coefficient,

$$\alpha_L(T) = \frac{1}{3V}\left[\frac{\partial V(T)}{\partial T}\right]_P \quad [6]$$

For the purpose of modeling high-temperature properties of materials, a standard SGTE polynomial form of the free energy is used to store information in thermodynamic databases:

$$G(T) = A + BT + CT\ln T + DT^2 + ET^{-1} + FT^3 \quad [7]$$

where *A, B, C, D, E* and *F* are constants for any fixed composition. That form is consistent with

$$H(T) = A - CT - DT^2 + 2ET^{-1} - 2FT^3 \quad [8]$$

and

$$Cp(T) = -C - 2DT - 2ET^{-2} - 6FT^2 \quad [9]$$

The polynomials [8] and [9] are often used to fit experimental calorimetry data. For low temperatures, however, Debye or Einstein models for heat capacity are more appropriate. The enthalpy and the entropy can be calculated by integration of the heat capacity data, using

$$H(T) = \int_{T^{\text{ref}}}^{T} Cp(T')dT' \quad [10]$$

$$S(T) = \int_{T^{\text{ref}}}^{T} \frac{Cp(T')}{T'}dT' \quad [11]$$

The free energy is then calculated using Eq. [1]. The experimental and theoretical thermodynamic data rarely form a self-consistent set. In order to determine the uncertainty associated with the data, we evaluated the properties of all Pu phases, as published in the literature. The analysis was based on Bayesian statistic combined with a Genetic Algorithm optimization technique.[18] Figure 16 shows the Gibbs free energy of the Pu condensed phases that was employed for the phase stability calculations.

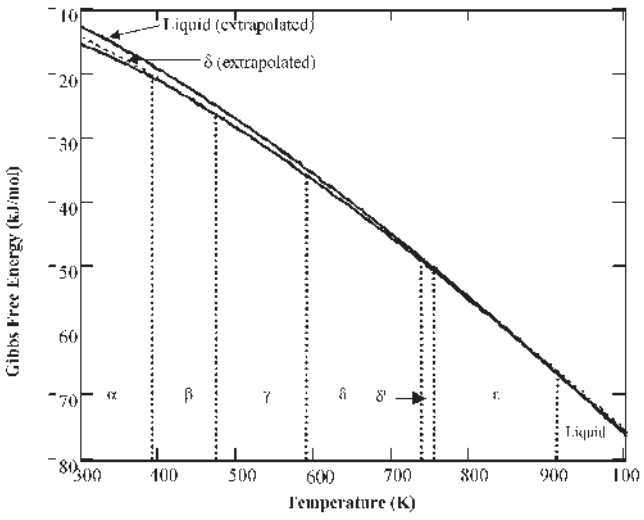

Fig. 16—Gibbs free energy of Pu phases. The free energy of each phase was extrapolated outside the stability intervals to calculate the equilibrium phase diagram.

The free energy of a Pu-Ga solution at constant pressure depends on temperature, the free energy of the components, $G_{\text{Pu}}(T)$ and $G_{\text{Ga}}(T)$, and the Ga atomic fraction x:

$$G(T,x) = G_{\text{Pu}}(T)(1-x) + G_{\text{Ga}}(T)x + k_B T[(1-x)\ln(1-x) + x\ln(x)] + G^{ex}(T,x) \quad [12]$$

where k_B is the Boltzmann constant, and the excess free energy G^{ex} can be approximated either by a Redlich–Kister polynomial with n terms,

$$G^{ex}(T,x) = x(1-x)\cdot\sum_{k=0}^{n} L_k(T)\cdot(1-2x)^k \quad [13]$$

where

$$L_k(T) = a_k + b_k T + c_k T\ln T + d_k T^2 \quad [14]$$

or by an equivalent quasi-chemical description,

$$G^{ex}(T,x) = x(1-x)\cdot\sum_k \left(\Omega_k^A(T)\cdot(1-x)^k + \Omega_k^B(T)\cdot x^k\right) \quad [15]$$

where again

$$\Omega_k(T) = a_k + b_k T + c_k T\ln T + d_k T^2 \quad [16]$$

For each fixed composition x, at constant pressure, thermodynamic relationships similar to the ones valid for pure component (Eqs. [1] through [6], [10], and [11]) must still hold. The chemical potential of the two components in the δ phase was calculated using

$$\mu_{\text{pu}}^{\delta}(T,x) = G^{\delta}(T,x) - x\left[\frac{\partial G^{\delta}(T,x)}{\partial x}\right]_{T,P} \quad [17]$$

$$\mu_{\text{Ga}}^{\delta}(T,x) = G^{\delta}(T,x) + (1-x)\left[\frac{\partial G^{\delta}(T,x)}{\partial x}\right]_{T,P} \quad [18]$$

At equilibrium, the chemical potential of each component must be the same in all phases that are present in the equilibrium configuration. For example, if the two phases in equilibrium are δ and α, then

$$\mu^{\delta}_{\mathrm{Pu}}(T, x) = \mu^{\alpha}_{\mathrm{Pu}}(T, x)$$
$$\mu^{\delta}_{\mathrm{Ga}}(T, x) = \mu^{\alpha}_{\mathrm{Ga}}(T, x) \qquad [19]$$

The system of Eq. [19] is equivalent with constructing the common tangent to the graphics of the free energies, at each fixed temperature.

One could prove that an equivalent representation of phase stability can be achieved using a pseudobinary system, such as Pu-Pu_3Ga. This representation, which is not a complete assessment of the phase diagram, is used to emphasize the relative stability of phases in the low Ga content area. Figure 17 shows the Gibbs free energy of selected phases in this system. In the pseudobinary system, the Gibbs free energy interaction parameters (Eqs. [15] and [16]) are temperature independent:

$$\Omega_{\mathrm{Pu}} = -42\ \Omega_{\mathrm{Pu_3Ga}} = -102\ (\mathrm{kJ/mol}) \qquad [20]$$

The free energy of the cubic Pu_3Ga compound phases was kept constant in the simulation:

$$G_{\mathrm{Pu_3Ga_{cubic}}}(T) = 15.158 - 0.187 \cdot T\ (\mathrm{kJ/mol}) \qquad [21]$$

The free energy of the tetragonal phase was determined by means of a relative free-energy parameter:

$$\Delta G_{\mathrm{Pu_3Ga}}(T) = -74.2 - 0.0138 \cdot T\ (\mathrm{kJ/mol}) \qquad [22]$$

All free energies have been then referenced to the stable phases of the components. Figure 17(a) shows this set of free energies is consistent with a eutectoid point at T = 370 K and x = 32 pct Pu_3Ga (that is, 8 pct Ga). This result is consistent with the experimental diagrams by Chebotarev *et al*. and with the CALPHAD assessment by Adler. However, the model is extremely sensitive to the interaction parameters. Figure 18 shows that small changes in the values of Ω (Eq. [20]) (within the common errors of phase stability assessments) can lead to qualitative changes in the phase diagram, making the δ phase stable at room temperature, as described in the Ellinger *et al*. diagram. The thermodynamic properties of the Pu_3Ga compound also play a critical role and changes in Eq. [22] qualitatively modify the phase diagram.

A thermodynamic treatment of the phase stability in the Pu-Ga system can also incorporate results from first principles and molecular dynamics calculations. The main result is usually the enthalpy of various phases, which is related to the free energy by

$$H(T) = G(T) - T\left[\frac{\partial G(T)}{\partial T}\right]_P \qquad [23]$$

The free energy is calculated by temperature integration, using the Gibbs–Helmholtz relationship:

$$\frac{G(T)}{T} = \frac{G^{\mathrm{ref}}(T^{\mathrm{ref}})}{T^{\mathrm{ref}}} - \int_{T^{\mathrm{ref}}}^{T} \frac{H(T)}{T^2}\, dT \qquad [24]$$

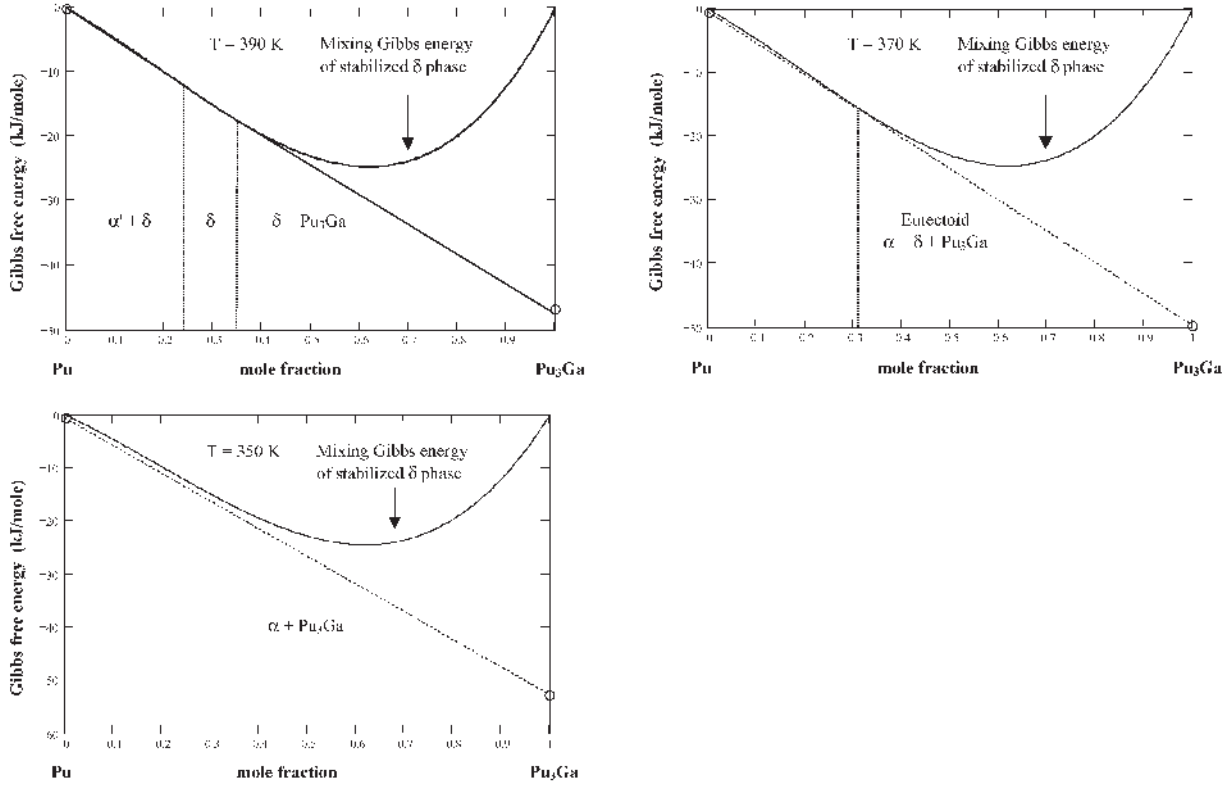

Fig. 17—Stability of phases in the Pu-Pu_3Ga system. Three phases are in equilibrium at 370 K, defining the eutectoid point. There is a stability interval of the δ phase above the eutectoid point (T = 390 K) and the δ phase decomposes into α + Pu_3Ga below the eutectoid point (T = 350 K).

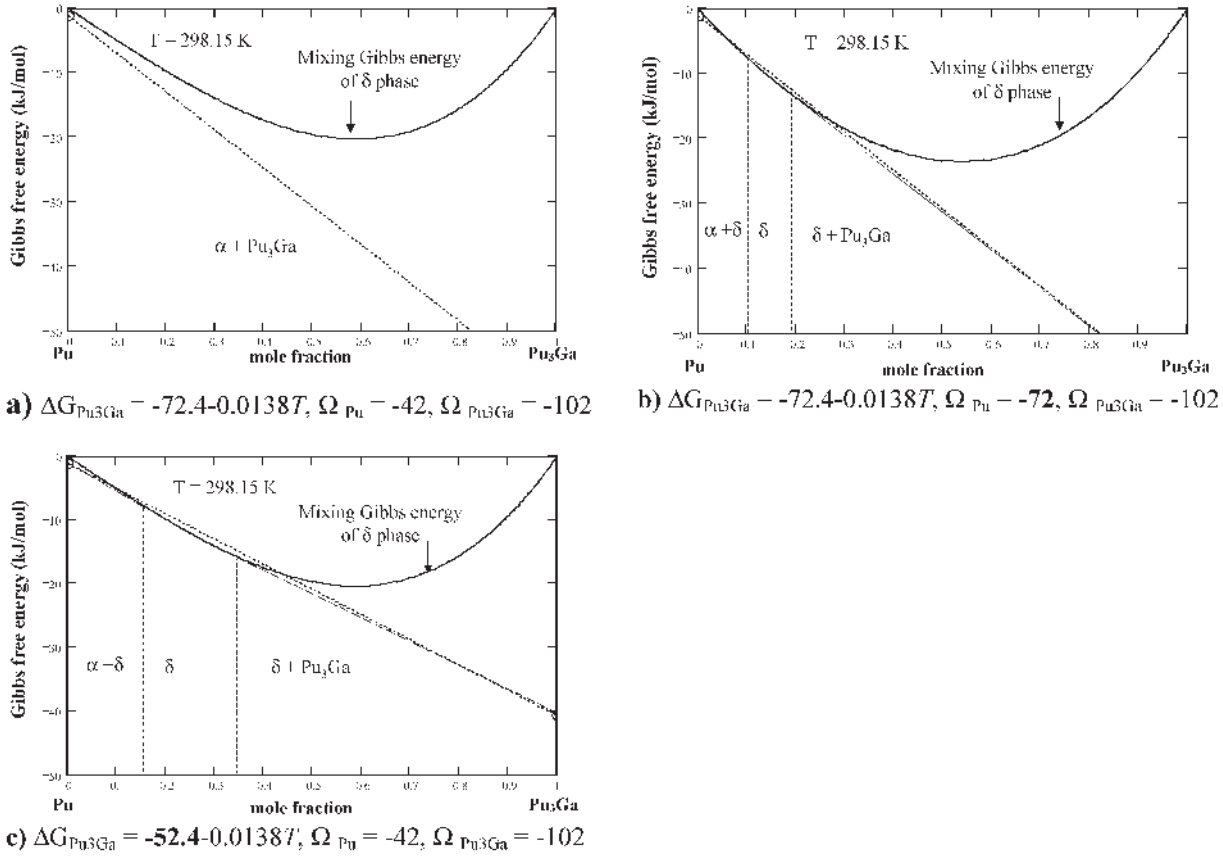

Fig. 18—The influence of model parameters on the stability of phases at room temperature. (*a*) The parameters defining the eutectoid point determined the $\alpha + Pu_3Ga$ configuration at room temperature. (*b*) and (*c*) Small changes in the parameter values changed the equilibrium configuration, allowing for the δ phase to be stable all the way to the room temperature.

The enthalpy values obtained by molecular dynamics calculations have been fitted using the polynomial functions described in Eq. [7] and [12]. The resulting phase diagram shows that the eutectoid is present and the room-temperature equilibrium configuration is a mixture of α plutonium and Pu_3Ga.

VII. CONCLUSIONS

This work summarizes recent efforts to develop a database of physical and transformation properties that is integrated with modeling efforts to elucidate the Pu-Ga phase diagram. In high-purity, zone-refined α Pu, we have found that the $\gamma \rightarrow \delta$ transformation is conventional, whereas the reversion is martensitic; that the $\gamma \rightarrow \beta$ cooling transformation is very sluggish; that heat release on cooling is less than that absorbed on heating; and that some γ is probably retained to room temperature. In Pu-Ga alloys, we found that dilatometry clearly resolves the martensitic nature of the $\alpha' \rightarrow \delta$ reversion; that there is a reinitiation of transformation during warming in Pu-0.5 wt pct Ga; and that there is a strong grain size effect on the $\delta \rightarrow \alpha'$ transformation temperature. Our modeling efforts show that the calculated Pu-Ga phase diagram is very sensitive to the thermodynamic properties of the compounds and to the excess free energy interaction parameters of solutions. Additionally, recent molecular dynamics calculations using the MEAM potential are consistent with the presence of a eutectoid point in the low-temperature, low Ga content area. Finally, it is too early to say that the equilibrium phase diagram is due to the large range and uncertainty in the experimental data, and that more experimental and theoretical work is necessary.

AKNOWLEDGMENTS

The authors thank Ramiro Pereyra and Darryl Lovato for their superb metallography, Mike Ramos for his thermomechanical processing expertise, and Jason Lashley for samples of the zone-refined alpha Pu. We also thank Sig Hecker, Tom Zocco, and Mike Baskes for insightful discussions. JNM thanks TEM for a lifetime of support and guidance. This project was funded by the United States Department of Energy under Contract No. W-7405-ENG-36.

REFERENCES

1. S.S. Hecker and L. Timofeeva: *Los Alamos Science*, 2000, vol. 26, pp. 244-51.
2. E.F. Hammel: *Plutonium Metallurgy at Los Alamos, 1943–1945: Recollections of Edward A. Hammel*, Los Alamos National Laboratory, Los Alamos, NM, 1998.
3. D.W. Ferrera, H.J. Doyle, and M.R. Harvey: RFP-1800, Rocky Flats Division, Dow Chemical U.S.A., Golden, CO, 1972.

4. H.R. Gardner: BNWL-13, Battelle-Northwest Laboratory, Richland, WA, 1965.
5. J. Mitchell, F. Gibbs, T. Zocco, and R. Pereyra: *Metall. Mater. Trans. A*, 2001, vol. 32A, pp. 649-59.
6. T.G. Zocco, D.S. Schwartz, J.C. Lashley, and J.N. Mitchell: Los Alamos National Laboratory, Los Alamos, NM, unpublished research, 2003.
7. R. Pascard: *Plutonium 1960*, Grenoble, France, 19-22 April, Cleaver-Hume Press, Ltd., London, 1960.
8. J.T. Orme, M.E. Faiers, B.J. Ward, H. Blank, and R. Linder: *5th Int. Conf. on Plutonium and Other Actinides 1975*, Baden-Baden, West Germany, 10-13 September, North-Holland, New York, 1975.
9. T. Zocco, M. Stevens, P. Adler, R. Sheldon, and G. Olson: *Acta Metall. Mater*., 1990, vol. 38, pp. 2275-82.
10. F. Ellinger, C. Land, and V. Struebing: *J. Nucl. Mater*., 1964, vol. 12, pp. 226-36.
11. B. Hocheid, A. Tanon, S. Bedere, J. Despres, S. Hay, and F. Miard: *Plutonium 1965: Proc. 3rd Int. Conf. on Plutonium*, Chapman and Hall, London, 1965.
12. N.T. Chebotarev, E.S. Smotriskaya, M.A. Andrianov, O.E. Kostyuk, H. Blank, and R. Linder: *5th Int. Conf. on Plutonium and Other Actinides 1975*, North-Holland Publishing Co., New York, NY, 1975, pp. 37-46.
13. M.E. Kassner and D.E. Peterson: *Binary Alloy Phase Diagrams*, 1986, vol. 1, p. 156.
14. D.E. Peterson and M.E. Kassner: *Binary Alloy Phase Diagrams*, 1986, vol. 2, pp. 1155-57.
15. P.H. Adler: *Metall. Mater. Trans. A*, 1991, vol. 22A, pp. 2237-46.
16. M.I. Baskes and M. Stan: *Metal. Mater. Trans. A*, 2003, vol. 34A, pp. 435-39.
17. M.I. Baskes, K. Muralidharan, M. Stan, S.M. Valone, and F.J. Cherne: *J. Met*., 2003, vol. 55, pp. 41-50.
18. M. Stan and B.J. Reardon: Los Alamos National Laboratory, Los Alamos, NM, unpublished research, 2003.
19. J.W. Ward: *Handbook on the Physics and Chemistry of the Actinides*, Elsevier Science Pub. Co., Amsterdam, 1986, pp. 332-41.
20. R. Pascard: *Plutonium 1960*, Cleaver-Hume Press Ltd., London, 1961.